The crystal structure of methane B at 8 GPa—An α-Mn arrangement of molecules

H. E. Maynard-Casely,[a] L. F. Lundegaard, I. Loa, M. I. McMahon, E. Gregoryanz, R. J. Nelmes, and J. S. Loveday
SUPA, School of Physics and Astronomy and Centre for Science at Extreme Conditions, The University of Edinburgh, Edinburgh EH9 3JZ, United Kingdom

(Received 5 September 2014; accepted 29 October 2014; published online 18 December 2014)

From a combination of powder and single-crystal synchrotron x-ray diffraction data we have determined the carbon substructure of phase B of methane at a pressure of ~8 GPa. We find this substructure to be cubic with space group $I\bar{4}3m$ and 58 molecules in the unit cell. The unit cell has a lattice parameter $a = 11.911(1)$ Å at 8.3(2) GPa, which is a factor of $\sqrt{2}$ larger than had previously been proposed by Umemoto *et al.* [J. Phys.: Condens. Matter **14**, 10675 (2002)]. The substructure as now solved is not related to any close-packed arrangement, contrary to previous proposals. Surprisingly, the arrangement of the carbon atoms is isostructural with that of α-manganese at ambient conditions.
 [http://dx.doi.org/10.1063/1.4903813]

I. INTRODUCTION

The behaviour of simple molecular systems under pressure provides a means to explore the density dependence of inter-molecular interactions, which gives insight of fundamental importance.[1] In the ice series HF, H_2O, NH_3, and CH_4, methane is the sole member that does not form hydrogen bonds in its solid phases. Its structures are therefore determined by the interplay of van der Waals interactions and steric effects. On compression at room temperature, methane crystallises at 1.5 GPa to form methane I. Methane I has a face-centred cubic (fcc) structure where the methane tetrahedra are thought to exhibit complete spherical orientational disorder.[2] The individual molecules have therefore been treated as spheres in previous studies and, as a result, the higher-pressure structures of solid methane have been discussed in terms of a "bad rare gas" model.[3–5] This has led to assumptions that methane's structural progression would be towards hexagonal-close packing (hcp) at high pressures above 25 GPa.[6] The progression to a hcp structure in solid methane was questioned when the high-pressure phase methane B was proposed to have cubic unit cell,[7] but this has remained unconfirmed.

Methane also makes up a significant fraction of both Uranus[8] and Neptune.[9] Detailed structural knowledge of solid high-pressure methane is therefore essential for the modelling and understanding of the complex phenomena that these planets exhibit. In Uranus and Neptune, methane is thought to exist within the "hot ice" layer from where the magnetic fields of these planets are proposed to originate.[10] These fields, which are non-axial and non-dipolar, are thought to be produced by "thin shell" convection within the ice layer. An understanding of the physico-chemical properties of the constituents of the "hot ice" layer is therefore crucial to models of the processes which generate these magnetic fields. For example, any dissociation of methane and subsequent precipitation of carbon, perhaps as diamond, would greatly influence the evolution and internal energy of these layers.[10] However, there is some debate on the conditions of the high-pressure dissociation of methane, where current simulations[11] and experimental results[12] contradict each other.

The current phase diagram of methane is set out in Figure 1. At 5.4 GPa and room temperature, methane transforms to methane A,[3] to which a rhombohedral structure has been assigned.[13] The structure of methane A has been fully determined with x-ray single crystal and neutron powder diffraction.[14] It has 21 molecules in a rhombohedral unit cell which are described by 39 different crystallographic sites for all the carbon and hydrogen atoms. The carbon atoms alone occupy 9 of these different sites. This previous study described how methane A is a heavily distorted variant of the cubic close-packed methane I.

Further compression results in another phase transition, which begins at 9 GPa on upstroke.[4] The phase above 9 GPa was originally named methane VII but has later been renamed methane B[6] to distinguish it from the low-temperature solid phases. To date, methane B has not been the subject of a full structural study and no atomic or molecular positions have been proposed. Its unit cell has been determined to be cubic with a lattice parameter of $a = 7.914$ Å at 16.9 GPa.[7] This simple cubic unit cell has been used to interpret a number of subsequent powder diffraction studies[15,16] and as a basis for computational studies.[17] A recent theoretical study claimed to have identified a cubic structure of methane with space group $I\bar{4}3m$ below 14 GPa from first-principle calculations,[18] but provided no lattice parameters or atomic co-ordinates for this structure.

Figure 1 shows that a further phase transition is thought to occur at 25 GPa and room temperature. This phase was called the hexagonal phase (HP) of methane and was thought

[a]Author to whom correspondence should be addressed. Electronic mail: helen.maynard-casely@ansto.gov.au. Present address: Bragg Institute, Australian Nuclear Science and Technology Organisation, Locked Bag 2001, Kirrawee DC, NSW, 2234, Australia.

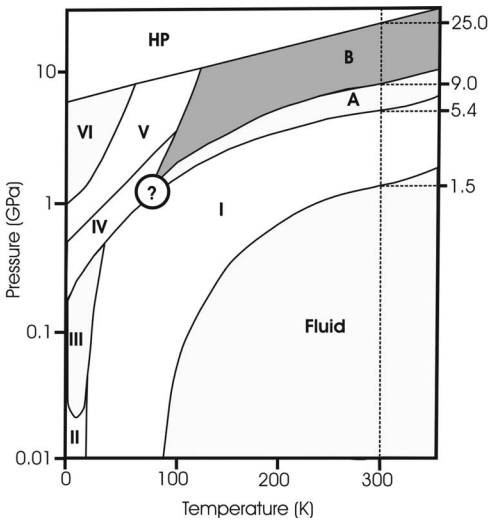

FIG. 1. The phase diagram of methane after Bini *et al.*[3] and the modifications of Umemoto *et al.*[7] The area marked with the question mark indicates where the phase boundaries have not yet been determined. The points marked to the right side of the diagram indicate the phase transition pressures (in GPa) at ambient temperature.

to be the "final" ordered hexagonally close-packed structure of solid methane.[6] On the basis of spectroscopic studies, Bini and Pratesi concluded that both methane HP and methane B have a single-site crystal structure, i.e., all molecular environments are identical.[3] To date, there have been limited structural studies on methane HP;[7,16] these dispute the assignment of a hexagonal structure to this phase as the diffraction patterns show close similarities to those of methane B.

Methane B occupies a substantial part of the phase diagram (see Figure 1) and is stable up to ∼25 GPa at room temperature. The conditions at the top of the ice layer of Uranus and Neptune are 20 GPa and 2000 K, so that methane B is the starting point for simulations of methane under the conditions found in this layer. Methane B is thus an important high-pressure phase. Knowledge of its structure would greatly improve understanding of planetary interiors and provide important insight into the nature of packing in simple molecular systems. In this paper we present the first detailed structural study of methane B using powder and single crystal synchrotron x-ray diffraction. Unlike in the study of methane A,[14] it has not proved possible to solve for the hydrogen positions. However, the carbon atom positions have all been determined, and thus the number of molecules per unit cell, which led us to revise the density of methane B at ∼8 GPa and revealed a surprising similarity to the structure of α–manganese.

II. SAMPLE PREPARATION AND DATA COLLECTION

For both the powder and single-crystal studies, Merrill-Bassett type diamond anvil pressure cells (MB cells)[19] were loaded cryogenically with research-grade methane from Sigma Aldrich (99.99% purity) and sealed within a rhenium gasket. The MB cells were equipped with Böhler-Almax seats and diamond anvils[20] to optimise access to reciprocal space and to avoid the background scattering from the beryllium backing plates that had been used in the original design of the MB cells.[19]

Pressures were measured with the ruby fluorescence method.[21,22] The small sample size and low x–ray scattering power of methane required the high flux of a synchrotron radiation source to collect high-quality diffraction data.

Previous work[5,14] indicates that it is difficult to obtain a good powder from a high-pressure methane sample, noting its tendency to form textured or large-grained powders. But we succeeded in obtaining a good powder of methane B from rapid compression to ∼20 GPa at ∼77 K, followed by sudden decompression. After warming to room temperature, the pressure of the sample was 8.0(2) GPa, within the down-stroke stability field of methane B as previously observed.[3] Powder x-ray diffraction data were collected on station ID09a at the European Synchrotron Radiation Facility (ESRF), Grenoble and are presented in Figure 2(a).

A single-crystal diffraction study was also undertaken. For this, methane was first cryogenically loaded into a MB cell, along with a ruby sphere for pressure determination, and when the cell had returned to room temperature, the pressure of the sample was increased to ∼10 GPa. To obtain single-crystals of methane B, the MB cell was externally heated to anneal the crystal grains of methane B that had formed on compression. Visual monitoring of the sample during heating showed that grain boundaries became more apparent at high temperature. As the melting temperature was approached, (at approximately 650 K at 10 GPa) the multiple grains of the sample were observed to anneal into a single crystal. This process was similar to that followed for the production of single crystals of methane A for a previous study,[14] but, unlike for methane A, it was found that it was not necessary to partially melt the sample to obtain good crystals of methane B. Following this process excellent crystals of methane B were produced giving reflections with typical rocking-curve width of 0.5°. The sample pressure was found to decrease on cooling to room temperature, so that resultant crystals of methane B stabilised at a pressure of ∼8 GPa at room temperature. X-ray diffraction data were subsequently collected on station 9.5 HPT at the Synchrotron Radiation Source (SRS) at Daresbury Laboratory,[23] and station ID09a at ESRF. The techniques developed to collect high-pressure single-crystal data at synchrotron facilities have been described elsewhere.[24,25]

Initial single-crystal x-ray diffraction data, shown in Figure 2(b), were collected on station 9.5 HPT at SRS, from a crystal at 8.3(2) GPa. The collection used an x-ray wavelength of 0.4439 Å and a mar345 image plate detector placed 340 mm from the sample. Data were collected out to a minimum d-spacing of 1.0 Å. The single-crystal diffraction images were collected as a sequence of contiguous 0.5° oscillations over a total scan range of ±35° around the vertical rotation axis. The exposure time of 20 s per frame was chosen to ensure that the strongest reflections did not saturate the detector. The cell was then rotated approximately 90° about the direction of the beam and the vertical rotation axis data collection was repeated. These data collections yielded 1578 non-saturated reflections, with all symmetry-equivalent reflections included in this count.

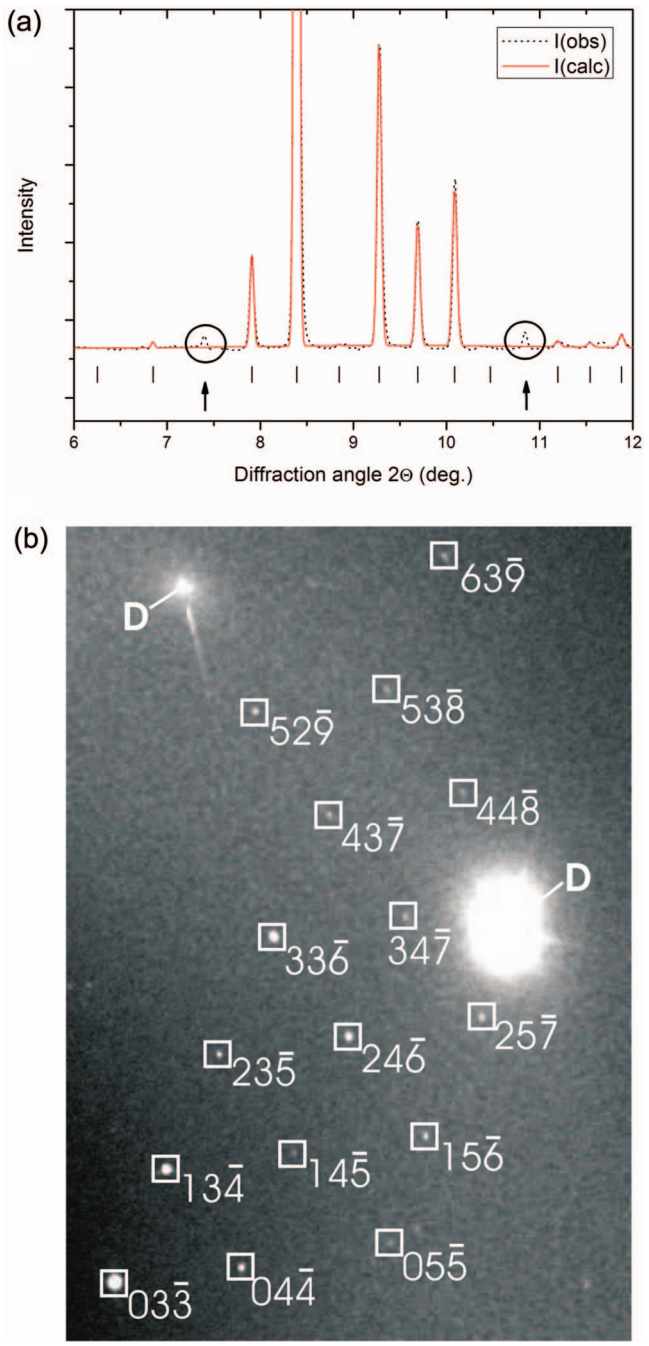

FIG. 2. Illustrations of the data used to solve the carbon substructure of methane B. (a) Powder diffraction profile of phase B at 8.0(2) GPa collected with x-rays of wavelength $\lambda = 0.4138$ Å. This has been fitted by the LeBail method[34] based on the unit cell of Umemoto *et al.*[7] suitably adjusted for the lower pressure. The tick marks below the profile indicate the calculated reflection positions. The circles highlight two peaks that are unexplained by this unit cell. (b) Composite image of single-crystal diffraction data collected at SRS from a crystal at 8.3(2) GPa, covering a rotation range of 3.5°. "D" marks diamond reflections. The Miller indices *hkl* shown by each reflection are based on a body-centred cubic lattice with lattice parameter $a = 11.994(3)$ Å.

A second data set was collected from a crystal at 7.9(2) GPa on station ID09a at the ESRF with a wavelength of 0.4131 Å and to a minimum *d*-spacing of 1.0 Å. These data were collected on a mar345 image plate detector in 0.35° contiguous oscillations over a scan range of ±35° around the vertical rotation axis, with an exposure time of 5 s per frame. Again, the cell was rotated around the horizontal axis by ∼90°, and the vertical rotation axis data collection was undertaken again. Because of the high x-ray flux on ID09a, a number of the reflections measured were saturated and had to be discarded. In total, these data collections measured 1226 non-saturated reflections.

III. SOLUTION OF THE CARBON SUBSTRUCTURE

Figure 2(a) shows a powder diffraction profile of methane B at 8.0(2) GPa. The unit cell that had previously been proposed for methane B, simple cubic with a lattice parameter of $a = 7.914$ Å at 16.9 GPa,[7] is not consistent with these data. Additional weak peaks, marked in Figure 2(a), suggest a larger cubic unit cell. We indexed this pattern based on a cubic cell with lattice parameter $a = 11.994(3)$ Å at 8.0(2) GPa, $\sqrt{2}$ larger than the unit cell parameter of Umemoto *et al.*[7] The systematic absences in the observed reflections (only reflections with $h + k + l = 2n$ are present) indicate that the lattice is body-centred. The increase in unit cell volume, by a factor of $2^{3/2}$, revises the estimated unit cell contents to ∼60 molecules. This large number of molecules prevented the structure from being solved from these powder diffraction data alone.

The single-crystal data sets were indexed with a body-centred cubic unit cell with $a = 11.850(2)$ Å for the data collected from the sample at 8.3(2) GPa at the SRS and $a = 11.911(1)$ Å for the data collected from the sample at 7.9(2) GPa at the ESRF. These values are consistent with the larger cubic cell deduced from the powder diffraction data and, after taking into account the unit-cell revision, those of Umemoto *et al.*[7] Examination of the observed reflections in both data sets also confirmed the body centring of the lattice, with $h + k + l = 2n$ for all observed reflections. Analysis of the intensities suggested $m\bar{3}m$ as the most likely Laue class. This additional information reduced the 1578 observed reflections in the SRS data, across the two data sets collected, to 186 unique reflections. Of these, 69 had intensities at least four times larger than their estimated standard deviations, $\sigma(I)$ [$I > 4\sigma(I)$] and these stronger reflections yielded an R_{merge} of 0.10 as a measure of the internal consistency of the data. Similarly, the 1226 reflections observed at ESRF across the two data collections reduced to 256 unique reflections with 76 of which had intensities four times greater than the estimated standard deviation and an R_{merge} of 0.13. Both data sets had reflections which violated the absences conditions of space group $I\bar{4}3d$; and hence the remaining four possible space groups consistent with the absences and the Laue group were $I432$, $I\bar{4}3m$, $Im\bar{3}m$ and $I4_132$. Structure solution was attempted in all four of these space groups using direct methods as implemented in SHELX.[26] The only plausible solutions for either data set were obtained with space group $I\bar{4}3m$.

The SRS data initially gave a solution with three independent atomic sites, which subsequently yielded the position of a fourth site for a carbon atom from examination of the Fourier difference maps. In the case of the ESRF dataset, the same four carbon atom positions were obtained from direct methods, and Fourier difference maps showed no evidence of any further carbon atoms. A refinement of the carbon-only substructure against squared structure factors, F^2, using the

TABLE I. Refined fractional coordinates of the centres of the methane tetrahedra (carbon atoms), and carbon atom atomic displacement parameters (see text), U_{iso}, of the methane B structure from a sample at 8.3(2) GPa, space group $I\bar{4}3m$, $a = 11.850(2)$ Å. The residuals of the refinement on $|F|^2$ using 69 unique reflections with $I > 4\sigma(I)$ were $wR(F^2) = 0.21$ and $wR(F) = 0.092$.

Atom	Wyckoff position	Site symmetry	x	y	z	U_{iso} (Å^2)
C1	2a	$\bar{4}3m$	0.000	0.000	0.000	0.10(7)
C2	24g	m	0.091(1)	0.091(1)	0.276(1)	0.09(1)
C3	8c	$3m$	0.320(2)	0.320(2)	0.320(2)	0.09(2)
C4	24g	m	0.145(2)	0.145(2)	0.533(3)	0.09(1)

SHELX software, gave weighted R factors of $wR(F^2) = 0.21$ and $wR(F) = 0.092$ for the SRS data set and $wR(F^2) = 0.20$ and $wR(F) = 0.089$ for the ESRF data set.

The refined co-ordinates obtained from the SRS dataset are shown in Table I. This structural arrangement contains carbon atoms (which also represent the molecular positions) generated by rotoinversion and hence it cannot be described in the chiral space groups $I432$ and $I4_132$. Similarly, space group $Im\bar{3}m$ would require the two 24g (x,x,z) sites to be related by an inversion centre, which they are clearly not. Thus the arrangement shown in Table I cannot be recreated in any of the other space groups allowed by the systematic absences and equivalences. Both data sets returned very similar carbon atom arrangements.

As for methane A, we sought the locations of the hydrogen atoms within the methane B structure. Unfortunately, in the case of methane B, neutron diffraction data were not available because in four attempts the CD_4 samples[27] did not transform to phase B, although the maximum pressure achieved (∼18 GPa) was well above the expected transformation pressure. As a result, we were not able to obtain an initial location for the H(D) atoms from neutron data as we were for phase A.[14] However, $F_{obs} - F_{calc}$ Fourier difference maps from the synchrotron x-ray single-crystal data did provide some suggestions for starting positions of the hydrogen

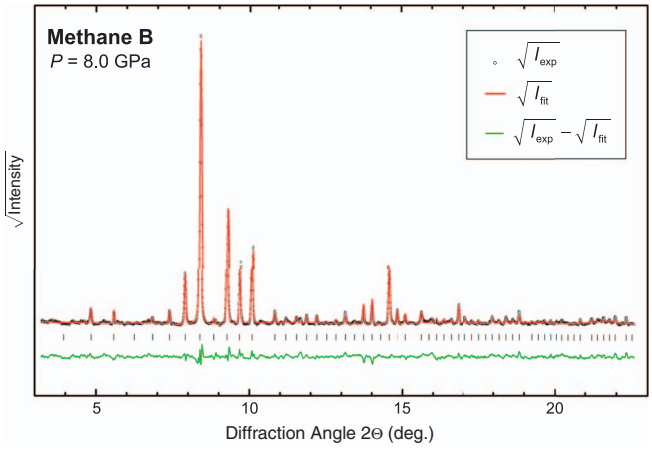

FIG. 3. Rietveld fit to the powder diffraction pattern shown in Fig. 2(a) using the carbon substructure determined from the single-crystal data. The square root of the intensities has been plotted, in order to present weaker features of the pattern. This fit yielded a weighted residual of $wRp = 5.5\%$.

TABLE II. Carbon fractional coordinates of methane B determined from the Rietveld refinement presented in Figure 3. The atomic displacement parameters (see text), U_{iso}, were constrained to be the same for all four sites.

Atom	x	y	z	U_{iso} (Å^2)
C1	0.000	0.000	0.000	0.089(4)
C2	0.0926(6)	0.0926(6)	0.2784(8)	0.089(4)
C3	0.3231(9)	0.3231(9)	0.3231(9)	0.089(4)
C4	0.1425(8)	0.1425(8)	0.5371(13)	0.089(4)

atoms. These were used with rigid body constraints in the GSAS program[28] to attempt to find molecular orientations. This approach proved unsuccessful and no physically plausible fit could be found. We are thus only able to present a determination of the heavy atom (carbon) substructure and not the full structure. As a result, it is not possible to rule out the possibility that the hydrogen atom positions break the $I\bar{4}3m$ symmetry, but on the basis of the evidence currently available there is no reason to propose such an effect.

The determination of the carbon substructure of methane B was further confirmed with a Rietveld refinement using the powder diffraction data presented in Figure 2(a). The Rietveld refinement was performed with the Jana 2006 program.[29] The fit, which is presented in Figure 3, gave a lattice parameter of $a = 11.9980(2)$ Å and atomic fractional coordinates, detailed in Table II, that are in excellent agreement with those determined from the single crystal data. In both cases, the U_{iso} values determined are larger than those determined previously for methane A.[14] This is not surprising as, unlike the structure determination of methane A, the hydrogen atoms have not been located, and so cannot be included separately in the refinement. The U_{iso} values include an additional amount that approximately accounts for the overall extent of the CH_4 molecule.

Interestingly, analysis of the carbon structure with the *TopasPro* software for topological analysis of crystal structures[30] reveals the surprising result that the complex arrangement of the 58 carbon atoms in the cubic unit cell corresponds to a known crystal structure – that of α-manganese at ambient conditions. The special positions occupied are identical to those of α-manganese and the atomic fractional coordinates given in Table I are within 0.01 of those of α-manganese.[31] This crystal structure has been described by Bradley and Thewlis[32] as well as Oberteuffer and Ibers.[31]

IV. DISCUSSION

Previous discussions of methane's structural transformation assumed that it would adopt the hcp structure at high pressure[4] and subsequent studies were interpreted on this basis.[3,6] This assumption was challenged by later work in which methane B was determined to have a cubic unit cell.[7] Our solution of the heavy-atom structure of methane B allows us to examine to what extent, if any, the structure can be described as close-packed.

Figure 4 shows the distribution of inter-molecular distances up to 12 Å for an ideal hcp, the methane A structure, and the methane B structure, all calculated with the same

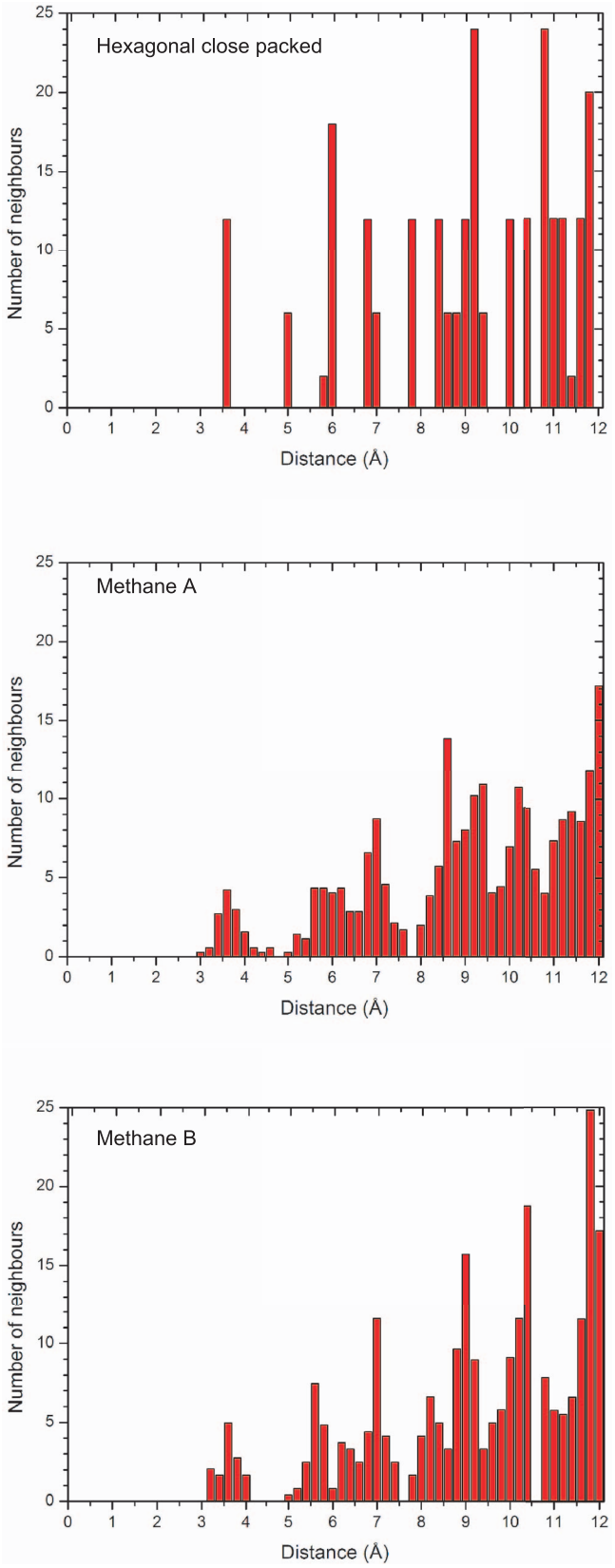

FIG. 4. The distribution of carbon to carbon distances in an ideal hexagonally close-packed structure, the methane A structure (as determined in Ref. 14) and the methane B structure, all with a molecular volume of 29.135 Å^3 molecule^{-1} (equivalent to methane B with a lattice parameter $a = 11.911$ Å) for distances up to 12 Å. The frequency of the distances in each of the graphs were averaged according to the multiplicity of each site, to enable a comparison to be made between the single-site structure (hcp), the nine-site structure (methane A), and the four-site structure (methane B).

molecular volume. As can be expected, there is a much more continuous distribution of distances in both methane A and B than in the hcp arrangement. Noticeable is the much larger distinction between the first- and second-neighbour shells in methane B compared to methane A. In methane B, there is a gap in the distribution of C–C distances in the range 4–5 Å whereas in methane A there is almost a continuous distribution of inter-molecular distances in this range. This pattern may also be seen for higher-order neighbours in that the methane B distribution is more tightly clustered than the distribution in methane A.

The cluster of inter-molecular distances can be examined more closely by separating them into the co-ordination shells around each of the four carbon atom sites. Figure 5 demonstrates the variety of C—C nearest-neighbour distances, which range from 3.140 to 3.888 Å at 8.3(2) GPa. The shorter distances (below 3.4 Å) are only associated with the C2 and C4 positions. As shown in Figure 5, there are quite large differences among the four co-ordination shells, suggesting significantly different molecular environments in the structure. The molecules at the C1 and C3 sites are situated in larger and more regular co-ordination shells, while the molecules located at the C2 and C4 positions are more restricted and have smaller and more distorted co-ordination shells.

Examination of the local co-ordination of the C2 position shows that it has twelve nearest neighbours. The C4 co-ordination shell is a distorted variant of the C2 co-ordination shell and has an additional neighbour, 13 in all. The C1 and C3 positions have 16 nearest neighbours. For C1, a high symmetry ($\bar{4}3m$) position, the co-ordination shell is a regular tetrahedral icosi-octahedron (a capping atom set on a six-member ring, over-topped by a six-member ring in a chair arrangement that is capped by a triangle). The C3 co-ordination shell is less constrained by symmetry and is a distorted tetrahedral icosi-octahedron. Closer examination of the C2 and C4 co-ordination shells reveals "cavities" in their co-ordination shells (as illustrated by the C2 coordination shell in Figure 5) where the molecular packing is distorted and allows room for the larger 16-member coordination shells of C1 and C3.

Both the methane A and methane B structures contain elements of 3-fold symmetry, perhaps imposed by the tetrahedral geometry of the methane molecule. Methane A, with its rhombobedral structure, has only one 3-fold symmetry axis, providing a greater freedom in the orientation of the methane molecules. As methane B is cubic, it has four axes of 3-fold symmetry, which places substantially more constraints on the molecular positions, and – assuming the full symmetry conforms to that of the carbon substructure determined here – on the molecular orientations. We see no evidence of distorted close-packed layers in methane B that we described in methane A.[14] Figure 4 demonstrates that the distorted close-packed structure of methane A has resulted in a spread of distances between carbon atoms in the structure. Methane B does not show such a pronounced spread of intermolecular distances, and the local co-ordination (see above) bears little, if any, relationship to a close-packed arrangement. This lack of close packing and range of different methane

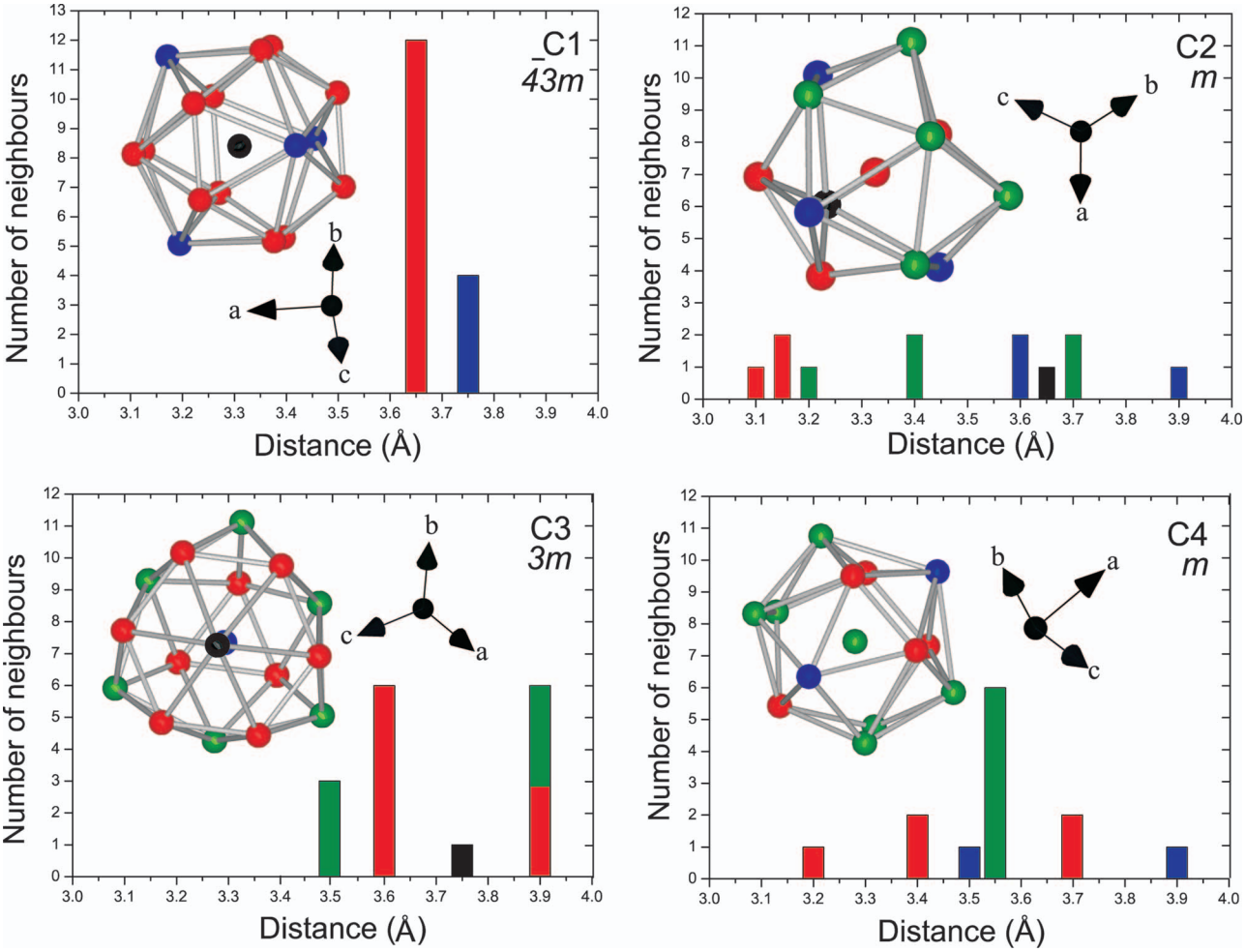

FIG. 5. The distribution of nearest-neighbour distances for the four different carbon atom sites in methane B at 8.3 GPa (Table I). The bars are coloured black for C1 atoms, red for C2, blue for C3, and green for C4. The site symmetry is shown top right in each panel. Thus, the C1 atom, on a site with $\bar{4}3m$ symmetry, has 12 C2 nearest neighbours and four C3. The corresponding co-ordination shell is shown top left in each panel, using the same colour coding, along with its orientation with respect to the unit cell axes.

environments might appear to be at odds with the relatively simple vibrational spectra in the internal mode region.[3,6,7] However, we note that in general internal modes are relatively insensitive to the molecular environment and are instead dominated by the internal molecular geometry which is unlikely to differ in the various methane phases.

We noted above that the arrangement of the molecules in methane B is the same as in the crystal structure of α-manganese, which appears surprising and remarkable. It may be significant that α-Mn orders magnetically on cooling[33] and that methane has nuclear spins associated with the protons. The large apparent deuteration effects we see for this transition (see above) may also be indicative of the nuclear spin (which is different for deuterons) having an effect on the crystal structure of methane B.

The structure of methane B would seem to have little structural relation with the preceding phase in pressure, methane A, which can be described as a distortion of a cubic close-packed structure.[14] The lack of a relationship between these two phases, and the complex structure of methane B we have described, suggests that a significant structural reconstruction occurs at the transition between methane A and B. This is reflected in the experimental evidence that the methane A to B transition is markedly "sluggish," being found to occur up to as high as 14 GPa on up-stroke and down to 6 GPa on down-stroke of pressure.[3,6]

V. CONCLUSIONS

Using synchrotron single-crystal and powder x-ray diffraction techniques, we have determined the carbon substructure of the high-pressure phase methane B. It has a body-centred cubic crystal lattice and a unit cell containing 58 CH_4 molecules. The complex arrangement of the carbon atoms is the same as in the cI58 crystal structure type of α-manganese.

Judging by the distribution of intermolecular distances, we conclude that the structure of methane B represents a departure from the pseudo close packing that was suggested by previous studies. The complex molecular arrangement of methane B appears to result from an increasing influence of the anisotropy of the methane molecules, and possibly also significant magnetic effect, as suggested above. This indicates the limitations of assuming a "bad rare gas" model for methane structures and the assumption that high-pressure

structures of methane would be variants of close-packed crystal structures.

ACKNOWLEDGMENTS

We would like to thank O. Degtyareva for assistance with the experiments as well as A. R. Lennie of beamline 9.5 HPT at Daresbury Laboratory and M. Hanfland of ID09a at the ESRF for their support. This work was supported by research grants, postgraduate funding (HEMC) and a fellowship (IL) from the U.K. Engineering and Physical Sciences Research Council, and facilities made available by the SRS and ESRF. Some of the experiments were conducted as part of the ESRF Long Term Project HS-3090 on Single-Crystal X-ray Diffraction at Extreme Conditions.

[1] A. F. Goncharov and R. J. Hemley, Chem. Soc. Rev. **35**(10), 899–907 (2006).
[2] W. Press, J. Chem. Phys. **56**, 2597 (1972).
[3] R. Bini and G. Pratesi, Phys. Rev. B **55**, 14800 (1997).
[4] P. Hebert, A. Polian, P. Loubeyre, and R. LeToullec, Phys. Rev. B **36**, 9196 (1987).
[5] R. M. Hazen, H. K. Mao, L. W. Finger, and P. M. Bell, Appl. Phys. Lett. **37**(3), 288 (1980).
[6] R. Bini, L. Ulivi, H. J. Jodl, and P. R. Salvi, J. Chem. Phys. **103**, 1353 (1995).
[7] S. Umemoto, T. Yoshii, Y. Akahama, and H. Kawamura, J. Phys.: Condens. Matter **14**, 10675 (2002).
[8] G. F. Lindal, J. R. Lyons, D. N. Sweetnam, V. R. Eshleman, D. P. Hinson, and G. L. Tyler, J. Geophys. Res.: Space Phys. **92**, 14987, doi:10.1029/JA092iA13p14987 (1987).
[9] B. A. Smith *et al.*, Science **246**, 1422 (1989).
[10] T. Guillot, Annu. Rev. Earth Planet. Sci. **33**, 493 (2005).
[11] F. Ancilotto, G. L. Chiarotti, S. Scandolo, and E. Tosatti, Science **275**, 1288 (1997).
[12] L. R. Benedetti, J. H. Nguyen, W. A. Caldwell, H. Lui, M. Kruger, and R. Jeanloz, Science **286**, 100 (1999).
[13] I. Nakahata, N. Matsui, Y. Akahama, and H. Kawamura, Chem. Phys. Lett. **302**, 359 (1999).
[14] H. E. Maynard-Casely, C. L. Bull, M. Guthrie, I. Loa, M. I. McMahon, E. Gregoryanz, R. J. Nelmes, and J. S. Loveday, J. Chem. Phys. **133**, 064504 (2010).
[15] L. L. Sun, W. Yi, L. Wang, J. F. Shu, S. Sinogeikin, Y. Meng, G. Shen, L. G. Bai, Y. C. Li, J. Liu, H. K. Mao, and W. L. Mao, Chem. Phys. Lett. **473**(1–3), 72–74 (2009).
[16] H. Hirai, K. Konagai, T. Kawamura, Y. Yamamoto, and T. Yagi, Chem. Phys. Lett. **454**(4–6), 212–217 (2008).
[17] L. Spanu, D. Donadio, D. Hohl, and G. Galli, J. Chem. Phys. **130**(16), 164520 (2009).
[18] H. Lin, Y. L. Li, Z. Zeng, X. J. Chen, and H. Q. Lin, J. Chem. Phys. **134**(6), 064515 (2011).
[19] L. Merrill and W. A. Bassett, Rev. Sci. Instrum. **45**, 290 (1974).
[20] R. Boehler and K. de Hantsetters, High Pressure Res. **24**, 391 (2004).
[21] G. J. Piermarini, S. Block, J. D. Barnett, and R. A. Forman, J. Appl. Phys. **46**, 2774 (1975).
[22] H. K. Mao and P. M. Bell, Science **191**(4229), 851–852 (1976).
[23] A. R. Lennie, D. Laundy, M. A. Roberts, and G. Bushnell-Wye, J. Synchrotron Radiat. **14**(5), 433–438 (2007).
[24] L. F. Lundegaard, C. Guillaume, M. I. McMahon, E. Gregoryanz, and M. Merlini, J. Chem. Phys. **130**(16), 164516 (2009).
[25] M. I. McMahon, I. Loa, G. W. Stinton, and L. F. Lundegaard, High Pressure Res. **33**(3), 485–500 (2013).
[26] G. M. Sheldrick, Acta Crystallogr. **64**, 112 (2008).
[27] Deuteration is required to eliminate the high background caused by incoherent neutron scattering from hydrogen atoms.
[28] A. C. Larson and R. B. Von Dreele, Los Alamos National Laboratory Report LAUR 86-748, 1994. Download a pdf from: https://subversion.xor.aps.anl.gov/EXPGUI/gsas/all/GSAS%20Manual.pdf.
[29] V. Petricek, M. Dusek, and L. Palatinus, Z. Kristallogr. **229**(5), 345–352 (2014).
[30] V. A. Blatov, A. P. Shevchenko, and D. M. Proserpio, Cryst. Growth Des. **14**(7), 3576–3586 (2014).
[31] J. Oberteuffer and J. Ibers, Acta Crystallogr., Sect. B: Struct. Crystallogr. Cryst. Chem. **26**(10), 1499–1504 (1970).
[32] A. Bradley and J. Thewlis, Proc. R. Soc. London, Ser. A **115**(771), 456–471 (1927).
[33] J. A. Oberteuffer, J. A. Marcus, L. H. Schwartz, and G. P. Felcher, Phys. Rev. B **2**(3), 670–677 (1970).
[34] A. Le Bail, Powder Diffr. **20**(4), 316–326 (2005).